

Structural and electrical transport properties of charge density wave material $LaAgSb_2$ under high pressure

Bowen Zhang(张博文), Chao An(安超), Xuliang Chen(陈绪亮), Ying Zhou(周颖), Yonghui Zhou(周永惠), Yifang Yuan(袁亦方), Chunhua Chen(陈春华), Lili Zhang(张丽丽), Xiaoping Yang(杨晓萍), and Zhaorong Yang(杨昭荣)
Citation: Chin. Phys. B, 2021, 30 (**7**): 076201. DOI: 10.1088/1674-1056/abf643
Journal homepage: http://cpb.iphy.ac.cn; http://iopscience.iop.org/cpb

What follows is a list of articles you may be interested in

Structural, mechanical, electronic properties, and Debye temperature of quaternary carbide Ti_3NiAl_2C ceramics under high pressure: A first-principles study

Diyou Jiang(姜迪友), Wenbo Xiao(肖文波), and Sanqiu Liu(刘三秋)
Chin. Phys. B, 2021, 30 (**3**): 036202. DOI: 10.1088/1674-1056/abca20

Utilizing of high-pressure high-temperature synthesis to enhance the thermoelectric properties of $Zn_{0.98}Al_{0.02}O$ with excellent electrical properties

Qi Chen(陈启), Xinjian Li(李欣健), Yao Wang(王遥), Lijie Chang(常立杰), Jian Wang(王健), Yuewen Zhang(张跃文), Hongan Ma(马红安), and Xiaopeng Jia(贾晓鹏)
Chin. Phys. B, 2021, 30 (**1**): 016202. DOI: 10.1088/1674-1056/abc4dd

Synthesis of black phosphorus structured polymeric nitrogen

Ying Liu(刘影)†, Haipeng Su(苏海鹏), Caoping Niu(牛草萍), Xianlong Wang(王贤龙), Junran Zhang(张俊然), Zhongxue Ge(葛忠学), and Yanchun Li(李延春)
Chin. Phys. B, 2020, 29 (**10**): 106201. DOI: 10.1088/1674-1056/aba9bd

Electronic structure and phase transition engineering in NbS_2: Crucial role of van der Waals interactions

Wei Wang(王威), Wen Lei(雷文), Xiaojun Zheng(郑晓军), Huan Li(黎欢), Xin Tang(唐鑫), Xing Ming(明星)
Chin. Phys. B, 2020, 29 (**5**): 056201. DOI: 10.1088/1674-1056/ab8214

Surperhard monoclinic BC_6N allotropes: First-principles investigations

Nian-Rui Qu(屈年瑞), Hong-Chao Wang(王洪超), Qing Li(李青), Yi-Ding Li(李一鼎), Zhi-Ping Li(李志平), Hui-Yang Gou(缑慧阳), Fa-Ming Gao(高发明)
Chin. Phys. B, 2019, 28 (**9**): 096201. DOI: 10.1088/1674-1056/ab3439

Structural and electrical transport properties of charge density wave material $LaAgSb_2$ under high pressure*

Bowen Zhang(张博文)[1,2], Chao An(安超)[3,4,†], Xuliang Chen(陈绪亮)[1,6], Ying Zhou(周颖)[3], Yonghui Zhou(周永惠)[1,6], Yifang Yuan(袁亦方)[1], Chunhua Chen(陈春华)[1], Lili Zhang(张丽丽)[5], Xiaoping Yang(杨晓萍)[1,6,‡], and Zhaorong Yang(杨昭荣)[1,3,6,§]

[1] *Anhui Province Key Laboratory of Condensed Matter Physics at Extreme Conditions, High Magnetic Field Laboratory, Chinese Academy of Sciences, Hefei* 230031, *China*

[2] *Science Island Branch, Graduate School of University of Science and Technology of China, Hefei* 230026, *China*

[3] *Information Materials and Intelligent Sensing Laboratory of Anhui Province, Institutes of Physical Science and Information Technology, Anhui University, Hefei* 230601, *China*

[4] *Key Laboratory of Structure and Functional Regulation of Hybrid Materials (Anhui University), Ministry of Education, Hefei* 230601, *China*

[5] *Shanghai Advanced Research Institute, Chinese Academy of Sciences, Shanghai* 200031, *China*

[6] *High Magnetic Field Laboratory of Anhui Province, Hefei* 230031, *China*

(Received 7 March 2021; revised manuscript received 5 April 2021; accepted manuscript online 9 April 2021)

Layered lanthanum silver antimonide $LaAgSb_2$ exhibits both charge density wave (CDW) order and Dirac-cone-like band structure at ambient pressure. Here, we systematically investigate the pressure evolution of structural and electronic properties of $LaAgSb_2$ single crystal. We show that the CDW order is destabilized under compression, as evidenced by the gradual suppression of magnetoresistance. At $P_C \sim 22$ GPa, synchrotron x-ray diffraction and Raman scattering measurements reveal a structural modification at room-temperature. Meanwhile, the sign change of the Hall coefficient is observed at 5 K. Our results demonstrate the tunability of CDW order in the pressurized $LaAgSb_2$ single crystal, which can be helpful for its potential applications in the next-generation devices.

Keywords: high pressure, charge density wave, crystal structure, electrical transport

PACS: 62.50.–p, 61.05.C–, 72.15.–v, 74.62.Fj **DOI:** 10.1088/1674-1056/abf643

1. Introduction

Rare-earth silver antimonides $RAgSb_2$ (R = La–Nd, Sm, Gd–Tm) have attracted intense interests due to their peculiar physical properties,[1–11] such as anisotropic magnetism,[2,3] Dirac-cone-like band structure,[6,7] and charge density wave (CDW) order.[9–11] Among these antimonides, $LaAgSb_2$ has been paid special attention to because it hosts both CDW and Dirac fermions.[7,9] $LaAgSb_2$ crystallizes in a simple tetragonal $ZrCuSi_2$-type structure ($P4/nmm$, No. 129), with La atoms intercalating between Sb and AgSb layers.[6–8] As temperature decreases, $LaAgSb_2$ experiences two CDW transitions at ~ 209 K and ~ 185 K, respectively.[12] The former transition corresponds to a periodic charge/lattice modulation along the a axis, while the latter one relates to a weaker modulation along the c axis.[9] Accompanying with the CDW transitions, striking anomalies have been observed in electrical transport, magnetic susceptibility, thermoelectric power, and infrared spectroscopy measurements.[1,8,13]

More recently, angle-resolved photoemission spectroscopy investigation and first-principle calculations consistently revealed that $LaAgSb_2$ possesses linear energy bands and a Dirac-cone-like structure near the Fermi level.[7] In particular, the segments of the Fermi surface pocket that is associated with the Dirac-cone-like structure are well nested with a small wave vector, documenting a close relationship of the Dirac cone to the CDW ordering.[7] Moreover, $LaAgSb_2$ exhibits a large linear magnetoresistance (MR) due to the existence of linear band dispersion, which disappears just above the CDW transition temperature of 207 K and provides additional evidence of the correlation between the Dirac cone and CDW ordering.[6,7] These unique properties make $LaAgSb_2$ a promising material for applications in CDW-based electronic devices.

Applying external pressure and chemical substitution are two effective ways to tune the CDW order.[10,11,14] Based on

*Project supported by the National Key Research and Development Program of China (Grant Nos. 2018YFA0305700, 2017YFA0403600, and 2016YFA0401804), the National Natural Science Foundation of China (Grant Nos. U1632275, U19A2093, U1932152, U1632162, 12004004, 11874362, 11804344, 11704387, and 11674325), the Natural Science Foundation of Anhui Province, China (Grant Nos. 1908085QA18, 2008085QA40, and 1808085MA06), the Users with Excellence Project of Hefei Science Center CAS (Grant Nos. 2018HSC-UE012, 2020HSC-CIP014, 2020HSC-UE015, and 2021HSC-UE008), and the Major Program of Development Foundation of Hefei Center for Physical Science and Technology (Grant No. 2018ZYFX002). A portion of this work was supported by the High Magnetic Field Laboratory of Anhui Province (Grant No. AHHM-FX-2020-02). Yonghui Zhou was supported by the Youth Innovation Promotion Association of Chinese Academy of Sciences (Grant No. 2020443).

†Corresponding author. E-mail: chaoan@ahu.edu.cn

‡Corresponding author. E-mail: xpyang@hmfl.ac.cn

§Corresponding author. E-mail: zryang@issp.ac.cn

© 2021 Chinese Physical Society and IOP Publishing Ltd

earlier studies, elements doping in both La and Ag sites disfavors the CDW in $LaAgSb_2$, which was partially attributed to the disorder generated by element substitution.[10,11] In contrast, without inducing additional impurities, applying external pressure provides a clean way for the modulation of the CDW. Previous electrical resistance measurements unveiled that the CDW is gradually suppressed by the applied pressure.[10,11,15] However, the highest pressure studied in the electrical transport measurements so far is limited to ~ 3.8 GPa.[15] How the CDW involves and whether novel phenomena can be induced at higher pressures are not clear and deserve further investigation.

Here, using pressure as a tuning knob, we systematically investigate the evolution of structural and electrical properties of $LaAgSb_2$ single crystals through *in-situ* synchrotron x-ray diffraction (XRD), Raman spectroscopy, and electrical transport measurements under pressures up to 41.6–49.0 GPa, combined with first-principles calculation. With increasing pressure, the magnetoresistance is monotonically suppressed and completely disappears at 21.5 GPa. In addition, at $P_C \sim$ 22 GPa, the sign change of the Hall coefficient is observed at 5 K. While no evident structural phase transition is observed via XRD, the simultaneous occurrence of c/a anomaly and new Raman peak unravels a structural modification at P_C.

2. Experimental details

Single crystals of $LaAgSb_2$ were grown by Sb self-flux method.[8] After removing the excessive Sb by centrifuging, plate-like crystals were obtained, as shown in the inset of Fig. S1(b). The temperature (T)-dependent electrical resistivity (ρ_{xx}) measurements at ambient pressure were conducted in a physical property measurements system (PPMS, Quantum Design Inc.).

High-pressure electrical transport measurements were conducted in a screw-pressure-type diamond anvil cell (DAC) made of Be–Cu alloy. The culet size of the diamond was 300 μm. The T301 stainless-steel gasket was pre-indented from thickness of 200 μm to 30 μm and a hole of about 280 μm was drilled in the center of the pit. Platinum foil served as the electrical contact. Soft NaCl fine powder was used as the pressure-transmitting medium (PTM). A piece of cleaved single crystal with dimensions of $\sim 100 \times 50 \times 10$ μm^3 together with some ruby powders was loaded into the chamber. $\rho_{xx}(T)$ curve was measured by using standard four-probe method. The current was introduced along the *ab* plane. Hall resistivity ρ_{xy} was measured at 5 K via five-probe method with external magnetic field along the *c* axis.

High-pressure powder x-ray diffraction experiments were conducted at beamline 15U1, Shanghai Synchrotron Radiation Facility (SSRF) at room temperature. Pressure was generated by a Mao–Bell type symmetric DAC. The culet of the diamond was 300 μm in diameter. The Re gasket was pre-indented to thickness of 30 μm and a hole of 150 μm was drilled as sample chamber. $LaAgSb_2$ powders were obtained by crushing and grinding the as prepared $LaAgSb_2$ single crystals. Pressed powder ($\sim 50 \times 50 \times 10$ μm^3) together with some ruby balls was loaded in the chamber. Daphne 7373 oil was used as the PTM. A focused monochromatic x-ray beam with wavelength 0.6199 Å was used for the angle-dispersive diffraction. The size of the focused x-ray beam at the sample position is 3 μm $\times$2.5 μm. Two-dimensional area detector Mar165 CCD was used to collect the powder diffraction patterns.[16] The detector was 185.88 mm away from the sample. The Dioptas[17] and Rietica programs[18] were employed for image integrations and structure refinement, respectively.

The high-pressure Raman spectrum measurement was performed at room temperature in a Mao–Bell type symmetric DAC using a commercial Renishaw Raman spectroscopy measurement system with a 532-nm laser excitation line. The diamond culet was 300 μm in diameter. The T301 stainless-steel gasket was pre-indented from thickness of 200 μm to 30 μm and a hole of about 150 μm was drilled as the sample chamber. Daphne 7373 oil served as the pressure medium. Pressure was calibrated by using the ruby fluorescence shift at room temperature for all above experiments.[19]

3. Results and discussion

Figure 1(a) displays the temperature-dependent resistivity $\rho_{xx}(T)$ measured at ambient pressure under 0 T and 14 T, respectively. One can see that accompanying with the formation of CDW order at around 210 K, the difference of resistivity $\Delta\rho = \rho_{xx}(H) - \rho_{xx}(0\ \mathrm{T})$ starts to develop and becomes pronounced with decreasing temperature, in accordance with previous reports.[6,8] Due to the simultaneous occurrence of CDW and $\Delta\rho$, the onset temperature of $\Delta\rho(T^*)$ is equal to the CDW transition temperature T_{CDW} at ambient pressure, see the inset of Fig. 1(a). To trace the evolution of CDW under compression, we measured the $\rho_{xx}(T)$ at each pressure under 0 T and 7 T, respectively. As seen from Figs. 1(b)–1(f), the $\Delta\rho$ is suppressed gradually with increasing pressure, meanwhile the T^* decreases monotonically. Both the suppression of $\Delta\rho$ and decrease of T^* are in line with the collapse of CDW order as reported in a previous study.[15] The $\Delta\rho$ eventually disappears at 21.5 GPa. However, it should be noted that the CDW order was found to be suppressed completely around ~ 3 GPa according to Ref. [15], which is much smaller than the critical pressure $P_C \sim 21.5$ GPa and may indicate the decoupling of $\Delta\rho$ and CDW order under high pressure. Meanwhile, as shown in Fig. S3, it can be seen that the linear range of MR is monotonically reduced upon compression and the whole curve can be fitted by a quadratic-field relation above P_C. In addition, ρ_{xx} maintains the metallic conduction behavior and no superconductivity is observed down to 1.8 K, see Fig. 1(g).

The resistivity at 300 K initially decreases with increasing pressure up to 5.1 GPa and then persistently increases upon further compression, accompanying with a sudden jump between 18.6 GPa and 21.5 GPa [Fig. 1(g)]. In general, the pressure enhances the band overlapping and the resistivity should decrease with increasing pressure. The abnormal enhancement of resistivity under high pressure could be attributed to different factors, such as non-hydrostatic compression, structural phase transition/electronic phase transition, and structural distortion.[20–24]

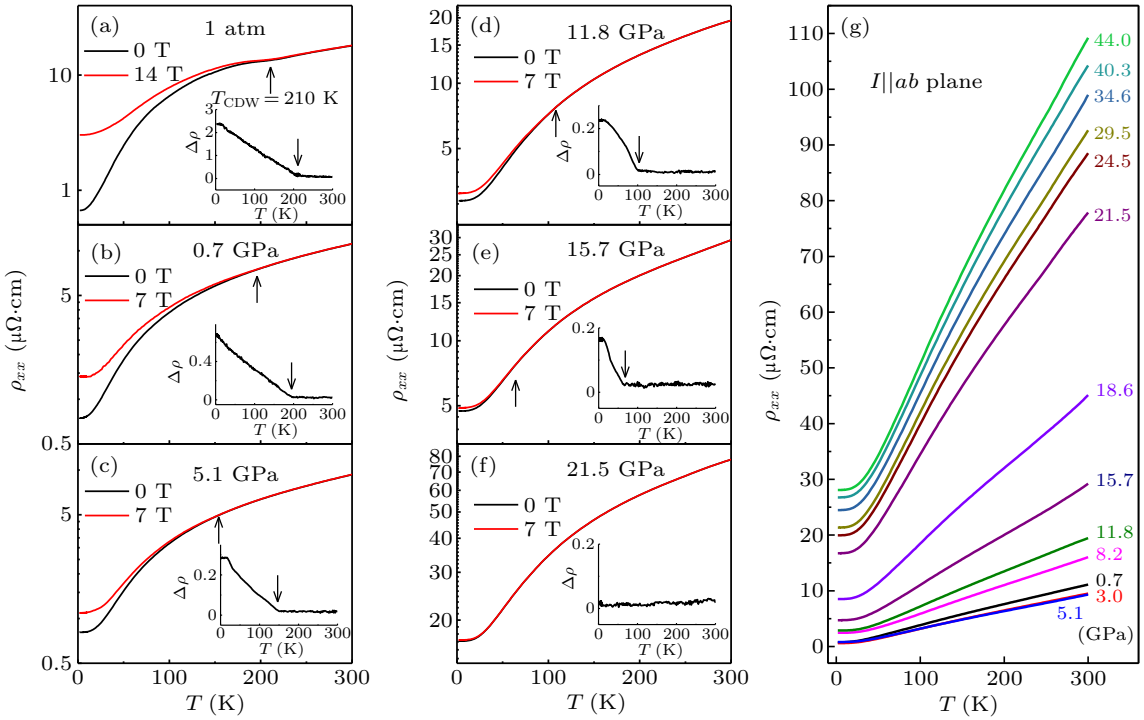


Fig. 1. (a)–(f) Temperature dependence of resistivity under 0 T (black line) and external magnetic field (red line) with H parallel to c axis at various pressures. Arrow marks the transition temperature T_{CDW} at ambient pressure and T^* under high pressure. The insets of (a)–(f) display temperature dependence of $\Delta\rho = \rho(H) - \rho(0\ \mathrm{T})$. (g) Temperature-dependent electrical resistivity of $LaAgSb_2$ in the pressure range of 0.7–44.0 GPa.

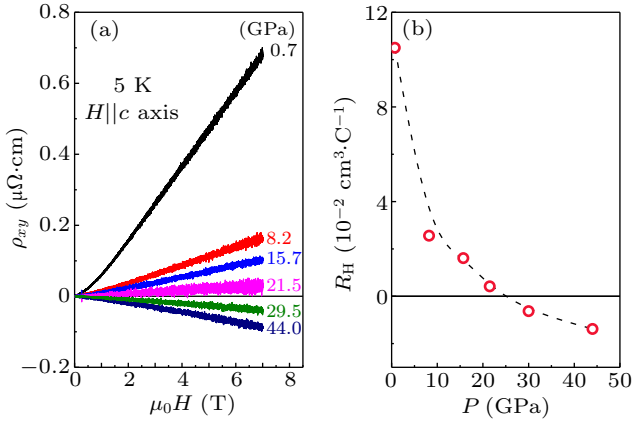


Fig. 2. (a) Field-dependent Hall resistivity ρ_{xy} of $LaAgSb_2$ single crystal under various pressures at 5 K with H parallel to c axis. (b) Pressure-dependent Hall coefficient R_H. The R_H is determined from the initial slope of ρ_{xy} at $H \to 0$.

Figure 2(a) displays the magnetic field (H)-dependent Hall resistivity $\rho_{xy}(H)$ at 5 K and various pressures. At 0.7 GPa, ρ_{xy} shows a quadratic field dependence in the low-field region while increases linearly at higher fields, consistent with the result at ambient pressure.[6] The nonmonotonic field dependence and positive slope of $\rho_{xy}(H)$ indicate that $LaAgSb_2$ exhibits a multiband feature and the hole-type carriers dominate the transport behavior. Hall coefficient R_H is extracted from the slope of $\rho_{xy}(H)$ around zero field, as displayed in Fig. 2(b). Upon compression, R_H decreases monotonically and changes into negative at pressures above 21.5 GPa. The sign change of R_H demonstrates that the hole-dominated conductivity maintains up to 21.5 GPa and is replaced by electron-dominated behavior at higher pressure. In general, the sign change of Hall coefficient directly reflects the modification of the Fermi surface, which could be caused by not only electronic phase transition,[25] but also the occurrence of structural instability.[26]

We further investigate the structural stability of $LaAgSb_2$ under high pressure via synchrotron XRD measurement. Figure 3(a) shows the XRD patterns at selected pressures. Upon compression, all Bragg peaks shift to larger angles due to the lattice shrinkage without appearing extra peaks up to 41.6 GPa. The XRD pattern at each pressure can be well indexed by the space group $P4/nmm$ (No. 129), see the representative refinements at 1.7 GPa and 41.6 GPa in Figs. 3(b) and 3(c). The volume versus pressure plotted in Fig. 3(d) is fitted by the third-order Birch–Murnaghan formula, which yields the ambient pressure volume $V_0 = 103.3(\pm 0.2)$ Å^3, bulk modulus $B_0 = 84.3(\pm 1.4)$ GPa with its first-order derivative B_0' being

fixed as 4. The extracted lattice parameters (a and c) are displayed in Fig. 3(f). Without detecting an evident structural transition, it can be seen that both a and c decrease monotonically with the applied pressure. Nevertheless, the axis ratio c/a, a measure of the relative compressibility along different crystal axis, displays a clear kink at around 22 GPa. On one hand, such a feature can be caused by non-hydrostatic compression due to the solidification of pressure transmitting medium.[27,28] However, we used Daphne 7373 as the pressure medium in the high pressure XRD measurement, which normally leads to the kink anomaly in lattice ratio c/a at around 7–8 GPa.[27,28] On the other hand, we notice that characteristic pressure of 22 GPa agrees well with the critical pressure where the Hall coefficient changes sign, which indicates that change in the electronic state could be correlated with the modification of lattice degree of freedom.

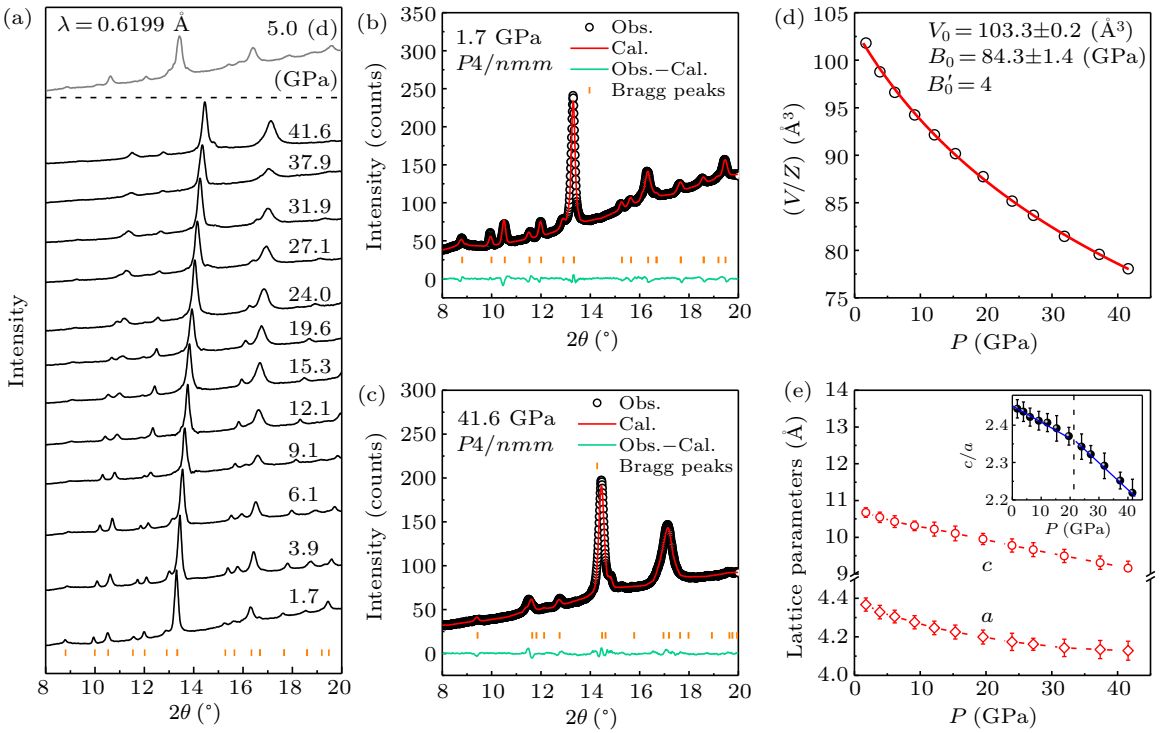


Fig. 3. (a) Synchrotron radiation x-ray diffraction patterns of $LaAgSb_2$ under various pressures ($\lambda = 0.6199$ Å). The XRD pattern upon decompression back to 5.0 GPa is denoted by d. (b), (c) The refinements at 1.7 GPa and 41.6 GPa were performed using RIETICA program with the Le Bail method. (d) The open symbols stand for unit volume. The solid red line is the fitting result based on the third-order Birch–Murnaghan equation of states. (e) Pressure dependence of the refined lattice parameters. The inset shows the lattice ratio of c/a as a function of pressure.

As an effective and powerful tool in detecting lattice vibrations, Raman scattering is sensitive to the local lattice symmetry and can provide information including electron–phonon coupling, weak lattice distortion, and structural transition.[29,30] For $LaAgSb_2$, a factor-group analysis yields a total number of 24Γ-point phonons, of which 12 ($4E_g \oplus 2A_{1g} \oplus 2B_{1g}$) are Raman-active modes, 9 ($3E_u \oplus 3A_{2u}$) are IR-active modes, and 3 ($E_u \oplus A_{2u}$) are acoustic modes. Both E_g and E_u are double degenerate modes. At ambient pressure (see Fig. S4(a) and Table SI in supplementary material), three prominent peaks with Lorentzian line shape are observed at $\sim$ 98.7 GPa, $\sim$ 108.1 GPa, and $\sim$ 126.3 GPa, which can be assigned to B^1_{1g}, A^1_{1g}, and A^2_{1g} Raman vibrational modes, respectively. As displayed in Fig. S4(b), all these Raman modes represent out-of-plane atomic vibrations, with B_{1g} involving Ag and Sb1 atoms while A_{1g} involving La and Sb2 atoms. Figure 4 shows the room-temperature Raman spectra at various pressures up to 49.0 GPa. One can see that all three Raman modes move towards higher frequencies monotonically with increasing pressure. Strikingly, in line with the appearance of c/a anomaly, a new peak (labeled as N) starts to appear at ca. 22.1 GPa and becomes prominent upon further compression. In principle, the emergence of new Raman modes normally involves a crystal symmetry breaking.[31–33] However, the XRD measurement indicates that the original tetragonal structure is maintained upon compression across the critical pressure. The discrepancy could be attributed to different sensitivity of the two methods. Comparing with XRD that is determined by the periodicity of crystal lattice, Raman spectrum depends on the point group symmetry and probes the structure on a local scale. Without detecting an evident structural transition by XRD, the simultaneous occurrence of c/a anomaly and new Raman peak is reminiscent of a pressure-induced structural modification, such as isostructural transition or a weak structural phase transition.[34–41] Especially, if the lattice structure of the new phase is very similar to the ini-

tial one, this transition will be too weak to be detected due to peak broadening of XRD pattern under pressure. In addition to the appearance of the new Raman peak, the structural modification is also reflected in the pressure dependences of other Raman modes plotted in Fig. 5(a), which demonstrate slope changes around 22 GPa. Meanwhile, the full width at half maximum (FWHM) of A_{1g}^2 mode decreases initially and displays a minimum around P_C [Fig. 5(b)], rather than broadens monotonically. Recalling the sign change of Hall coefficient at P_C, this structural modification should be the main reason.

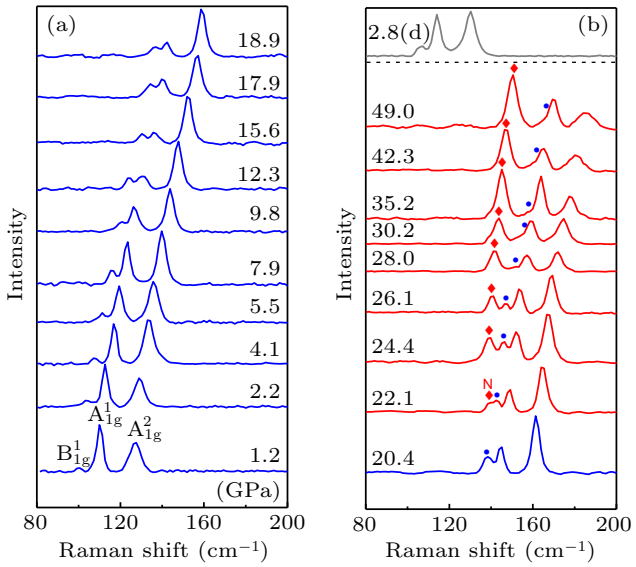


Fig. 4. Room-temperature Raman spectra of $LaAgSb_2$ single crystal in the pressure ranges of (a) 1.2–18.9 GPa and (b) 20.4–49.0 GPa, respectively. The blue solid dots and red diamonds indicate the appearance of new peak above 22.1 GPa. The Raman spectrum upon decompression back to 2.8 GPa is denoted by d.

After constructing a phase diagram in Fig. 5(c), a vivid correlation between the electrical and structural properties presents in the pressurized $LaAgSb_2$. The sign change of the Hall coefficient evidences the changes of the Fermi surface at P_C. As the CDW in $LaAgSb_2$ originates from nesting of segments of the Fermi surface pocket associated with the Dirac-cone-like structure, the collapse of CDW should be concomitant with the disappearance of Dirac fermions. Along with the modulation in the Fermi surface, the structural modification and an abrupt increment of room temperature resistivity are detected at the same critical pressure. Accordingly, a question arises as what is the origin behind these changes. On one hand, the modulation of electronic state could be attributed to the structural modification. On the other hand, the structural modification might be caused by the reconstruction of the Fermi surface, which accords with a scenario of electronic topological transition (ETT) or Lifshitz transition.[42] The ETT or Lifshitz transition does not require the structural transition, but normally leads to anomalies in the phonon spectrum or anomalies in c/a ratio.[43–47]

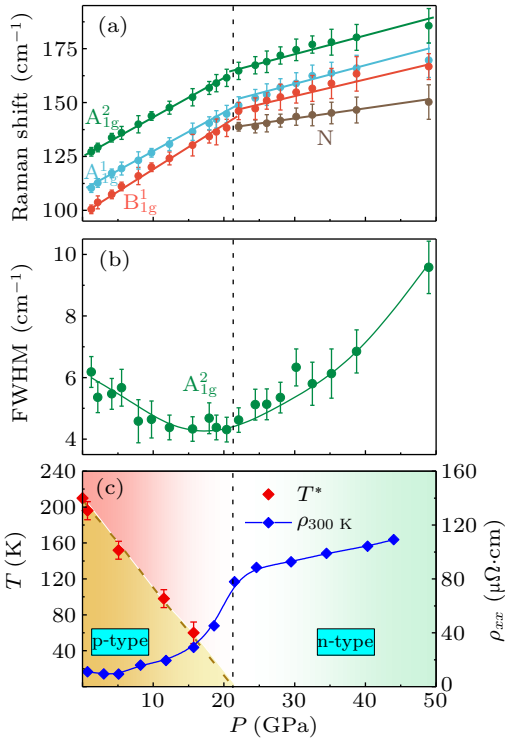


Fig. 5. (a) Pressure dependence of Raman frequencies of $LaAgSb_2$. Solid lines are linear fits to data. (b) FWHM of the A_{1g}^2 Raman mode as a function of pressure and solid line is drawn as guide to the eyes. (c) Pressure-temperature phase diagram of $LaAgSb_2$. The left axis stands for the temperature T and the right axis corresponds to the resistivity ρ_{xx}.

4. Conclusion

In summary, the pressure effects on structural and electronic properties of single crystal $LaAgSb_2$ were investigated by combining electronic transport, XRD, and Raman experiments. With increasing pressure, the magnetoresistance is suppressed gradually. Both XRD and Raman experiments consistently uncover a structural modification at $P_C = 22$ GPa. The structural modification is characterized by a kink anomaly in c/a and a newly appeared Raman mode, and is accompanied by the sign change in the Hall coefficient.

References

[1] Chen R Y, Zhang S J, Zhang M Y, Dong T and Wang N L 2017 *Phys. Rev. Lett.* **118** 107402
[2] Sidorov V A, Bauer E D, Frederick N A, Jeffries J R, Nakatsuji S, Moreno N O, Thompson J D, Maple M B and Fisk Z 2003 *Phys. Rev. B* **67** 224419
[3] Myers K D, Canfield P C, Kalatsky V A and Pokrovsky V L 1999 *Phys. Rev. B* **59** 1121
[4] Song C, Good W, Wermeille D, Goldman A I, Bud'ko S L and Canfield P C 2002 *Phys. Rev. B* **65** 172415
[5] Prozorov R, Vannette M D, Samolyuk G D, Law S A, Bud'ko S L and Canfield P C 2007 *Phys. Rev. B* **75** 014413
[6] Wang K F and Petrovic C 2012 *Phys. Rev. B* **86** 155213
[7] Shi X, Richard P, Wang K F, Liu M, Matt C E, Xu N, Dhaka R S, Ristic Z, Qian T, Yang Y F, Yang C, Shi M and Ding H 2016 *Phys. Rev. B* **93** 081105
[8] Myers K D, Bud'ko S L, Fisher I R, Islam Z, Kleinke H, Lacerda A H and Canfield P C 1999 *J. Magn. Magn. Mater.* **205** 27
[9] Song C, Park J, Koo J, Lee K B, Rhee J Y, Bud'ko S L, Canfield P C, Harmon B N and Goldman A I 2003 *Phys. Rev. B* **68** 035113

[10] Bud'ko S L, Wiener T A, Ribeiro R A, Canfield P C, Vogt T and Lacerda A H 2006 *Phys. Rev. B* **73** 184111

[11] Torikachvili M S, Bud'ko S L, Law S A, Tillman M E, Mun E D and Canfield P C 2007 *Phys. Rev. B* **76** 235110

[12] Watanabe Y, Inada Y, Hidaka H, Kotegawa H, Kobayashi T C, Matsuda T D and Aoki D 2006 *Physica B* **378–380** 827

[13] Mun E D, Bud'ko S L and Canfiel P C 2011 *J. Phys.: Condens. Matter* **23** 476001

[14] Yomo R, Yamaya K, Abliz M, Hedo M and Uwatoko Y 2005 *Phys. Rev. B* **71** 132508

[15] Akiba K, Nishimori H, Umeshita N and Kobayashi T C 2021 *Phys. Rev. B* **103** 085134

[16] Zhang L L, Yan S, Jiang S, Yang K, Wang H, He S M, Liang D X, Zhang L, He Y, Lan X Y, Mao C W, Wang J, Jiang H, Zheng Y, Dong Z H, Zeng L Y and Guo L A 2015 *Nucl. Sci. Tech.* **26** 060101

[17] Prescher C and Prakapenka V B 2015 *High Pressure Res.* **35** 223

[18] Hunter B A 1998 *Rietica — a Visual Rietveld Program*, International Union of Crystallography Commission on Powder Diffraction Newsletter No. 20 (Summer 1998) http://www.rietica.org.

[19] Mao H K, Xu J and Bell P M 1986 *J. Geophys. Res.* **91** 4673

[20] Zhou Y, Lu P, Du Y, Zhu X, Zhang G, Zhang R, Shao D, Chen X, Wang X, Tian M, Sun J, Wan X, Yang Z, Yang W, Zhang Y and Xing D 2016 *Phys. Rev. Lett.* **117** 146402

[21] Chen C H, Zhou Y H, Chen X L, Han T, An C, Zhou Y, Yuan Y F, Zhang B W, Wang S Y, Zhang R R, Zhang L L, Zhang C J, Yang Z R, Delong L E and Cao G 2020 *Phys. Rev. B* **101** 144102

[22] Zhang M, Wang X Q, Azizur Rahman, Zeng Q S, Huang D, Dai R C, Wang Z P and Zhang Z M 2018 *Appl. Phys. Lett.* **112** 041907

[23] Enderlein C, Ramos S M, Bittencourt M, Continentino M A, Brewer W and Baggio-Saitovich E 2013 *J. Appl. Phys.* **114** 143711

[24] Ma Y, Eremets M, Oganov A R, Xie Y, Trojan I, Medvedev S, Lyakhov A O, Valle M and Prakapenka V 2009 *Nature* **458** 182

[25] Guo J, Wang H H, Von Rohr F, Yi W, Zhou Y Z, Wang Z, Cai S, Zhang S, Li X D, Li Y C, Liu J, Yang K, Li A G, Jiang S, Wu Q, Xiang T, Cava R J and Sun L L 2017 *Phys. Rev. B* **96** 224513

[26] Zhou Y H, Chen C H, Zhou Y, Chen X L, Gu C C, An C, Zhang B W, Yuan Y F, Wu H, Zhang R R, Zhang L L, Zhu X D, Yang X P and Yang Z R 2019 *Phys. Rev. B* **99** 125104

[27] Kenichi T 1999 *Phys. Rev. B* **60** 6171

[28] Gu C C, Hu J, Chen X L, Guo Z P, Fu B T, Zhou Y H, An C, Zhou Y, Zhang R R, Xi C Y, Gu Q Y, Park C, Shu H Y, Yang W G, Pi L, Zhang Y H, Yao Y G, Yang Z R, Zhou J H, Sun J, Mao Z Q and Tian M L 2019 *Phys. Rev. B* **100** 205124

[29] Rajaji V, Dutta U, Sreeparvathy P C, Sarma S C, Sorb Y A, Joseph B, Sahoo S, Peter S C, Kanchana V and Narayana C 2018 *Phys. Rev. B* **97** 085107

[30] An C, Chen X L, Wu B, Zhou Y H, Zhou Y, Zhang R R, Park C Y, Song F Q and Yang Z R 2018 *Phys. Rev. B* **97** 174516

[31] Nakayama A, Aoki K and Carlón R P 2001 *Phys. Rev. B* **64** 064104

[32] Errandonea D, Manjón F J, Garro N, Rodríguez-Hernández P, Radescu S, Mujica A, Muñoz A and Tu C Y 2008 *Phys. Rev. B* **78** 054116

[33] Muthu D V S, Teredesai P, Saha S, Suchitra, Waghmare U V, Sood A K and Rao C N R 2015 *Phys. Rev. B* **91** 224308

[34] Boulova M, Rosman N, Bouvier P and Lucazeau G 2002 *J. Phys.: Condens. Matter* **14** 5849

[35] Zarechnaya E, Dubrovinskaia N, Caracas R, Merlini M, Hanfland M, Filinchuk Y, Chernyshov D, Dmitriev V and Dubrovinsky L 2010 *Phys. Rev. B* **82** 184111

[36] Pereira A L J, Gracia L, Santamaría-Pérez D, Vilaplana R, Manjón F J, Errandonea D, Nalin M and Beltrán A 2012 *Phys. Rev. B* **85** 174108

[37] Zhao Z, Wang S B, Zhang H J and Mao W L 2013 *Phys. Rev. B* **88** 024120

[38] Ibáñez J, Sans J A, Popescu C, López-Vidrier J, Elvira-Betanzos J J, Cuenca-Gotor V P, Gomis O, Manjón F J, Rodríguez-Hernández P and Muñoz A 2016 *J. Phys. Chem. C* **120** 10547

[39] Wang L R, Wang K, Xiao G J, Zeng Q S and Zou B 2016 *J. Phys. Chem. Lett.* **7** 5273

[40] Zhang L, Zeng Q X and Wang K 2017 *J. Phys. Chem. Lett.* **8** 3752

[41] Pal S, Arora R, Roychowdhury S, Harnagea L, Saurabh K, Shenoy S, Muthu D V S, Biswas K, Waghmare U V and Sood A K 2020 *Phys. Rev. B* **101** 155202

[42] Lifshitz I M 1960 *Sov. Phys. JPET* **11** 1130

[43] Vilaplana R, Santamaría-Pérez D, Gomis O, Manjón F J, González J, Segura A, Muñoz A, Rodríguez-Hernández P, Pérez-González E, Marín-Borrás V, Muñoz-Sanjose V, Drasar C and Kucek V 2011 *Phys. Rev. B* **84** 184110

[44] Vilaplana R, Gomis O, Manjón F J, Segura A, Pérezgonzález E, Rodríguez-Hernández P, Muñoz A, González J, Marín-Borrás V, Muñoz-Sanjosé V, Drasar C and Kucek V 2011 *Phys. Rev. B* **84** 104112

[45] Gomis O, Vilaplana R, Manjón F J, Rodríguez-Hernández P, Pérez-González E, Muñoz A, Kucek V and Drasar C 2011 *Phys. Rev. B* **84** 174305

[46] Bera A, Pal K, Muthu D V S, Sen S, Guptasarma P, Waghmare U V and Sood A K 2013 *Phys. Rev. Lett.* **110** 107401

[47] Rajaji V, Dutta U, Sreeparvathy P C, Sarma S C, Sorb Y A, Joseph B, Sahoo S, Peter S C, Kanchana V and Narayana C 2018 *Phys. Rev. B* **97** 085107